

SLAC-PUB-4828

January 1989

(T/E)

Results from MARK III on the J/ψ Decays^{*}

USHA MALLIK[†]

The University of Iowa, Iowa City, IA 52242

and

Stanford Linear Accelerator Center, Stanford, CA 94309

ABSTRACT

The MARK III detector at the SPEAR e^+e^- storage ring at SLAC accumulated a data sample of 5.8×10^6 J/ψ produced in 1982, '83 and '85. Recent results in radiative decays, including different decay modes of the η_c and the search for scalars, are presented. The systematic study of the hadronic decays of the J/ψ into a vector-tensor meson pair is discussed, and a detailed analysis of the decay mode $J/\psi \rightarrow \omega f_2(1270)$ is described.

*Invited talk presented at the meeting of
the BNL Workshop on Glueballs, Hybrids and Exotic Hadrons
at Brookhaven National Labs, Upton, New York,
August 29-September 1, 1988.*

^{*} Work supported in part by the Department of Energy, under contracts DE-AC03-76SF00515, DE-AC02-76ER01195, DE-AC03-81ER40050, DE-AM03-76SF0034, DE-AC02-87ER40318 and by the National Science Foundation.

[†] Representing the MARK III Collaboration.

1. INTRODUCTION

A real test of Quantum Chromodynamics (QCD) continues to be the existence of glueballs, *i.e.*, bound states of gluons. Lattice gauge theory predicts^[1] them to be in the mass region of 1–2.5 GeV/ c^2 and expects the lowest lying states to be $J^{PC} = 0^{++}$ and 2^{++} . It is also possible to have mixed states of quarks and gluons, called hybrid states. To identify these states, it is imperative to have a complete understanding of the ordinary meson spectroscopy; hence, the recent interest in glueballs, hybrids, exotics and meson spectroscopy. Radiative decays of the J/ψ , decay channels with double pomeron exchange mechanism and the Okubo–Zweig–Ikuho (OZI) suppression mechanism, have been the glue hunting ground. The mass regions of the two popular glueball candidates^[2,3] observed in the J/ψ decays, the $\eta(1440)$, and the $f_2(1720)$ have been extensively discussed at this conference. In presenting recent results from MARK III, I will concentrate on mass regions other than these. A complete status of the radiative vector vector decay modes is presented, with details of $\eta_c(2980)$ production. The search for a scalar state in the radiative decays is described. This was motivated by the predictions of lattice gauge theory of the existence of a scalar glueball in the mass range 1–1.4 GeV/ c^2 .^[1] Among the hadronic decays of the J/ψ , a systematic study of quark correlations and the amplitudes in the decay of the J/ψ into a vector tensor meson pair is discussed.

2. THE DECAY MODES $J/\psi \rightarrow \gamma + \text{VECTOR} + \text{VECTOR}$

The decay channels presented here are $J/\psi \rightarrow \gamma\phi\phi$, $\gamma K^*(892)^0 \bar{K}^*(892)^0$, $\gamma\pi^+\pi^-\pi^+\pi^-$, $\gamma\omega\phi$, and $\gamma\omega\omega$. For each of these decay modes, the $\eta_c(2980)$ region in the vector-vector mass spectrum is discussed. In addition, structures near threshold and the important features in the mass spectra were studied. For the η_c decays, these studies yield information regarding whether or not the decays are SU(3) symmetric. By comparing the relative rates it also sheds light on nature of the predominant decay mechanisms, as shown in Fig. 1.

$J/\psi \rightarrow \gamma\phi\phi$

This reaction was observed in two decay modes: (a) where both ϕ 's decay into K^+K^- and (b) where one ϕ decays into K^+K^- and the other ϕ decays into $K_S^0K_L^0$. Figures 2(a) and (b) show the efficiency corrected $\phi\phi$ reconstructed mass spectra (with the efficiency plotted over) for decay modes (a) and (b), respectively. The two mass spectra are very similar. The $\eta_c(2980)$ peak is prominent and above threshold, a broad structure is observed in each case. The mass and the width of the structure at ~ 2200 MeV/c² were measured as $M = 2224 \pm 16 \pm 4$ MeV/c², $\Gamma = 136 \pm 55 \pm 20$ MeV/c² and $M = 2214 \pm 23 \pm 5$ MeV/c², $\Gamma = 187 \pm 74 \pm 35$ MeV/c², respectively, for decay modes (a) and (b). The corresponding branching ratios were $B(J/\psi \rightarrow \gamma X) \cdot (X \rightarrow \phi\phi) = (3.9 \pm 1.0 \pm 0.8) \times 10^{-4}$, and $(3.0 \pm 0.8 \pm 0.6) \times 10^{-4}$. The decay branching ratio into $\eta_c(2980)$ for the two modes were measured as $B[J/\psi \rightarrow \gamma\eta_c(2980)] \cdot [\eta_c(2980) \rightarrow \phi\phi] = (0.96 \pm 0.2 \pm 0.14) \times 10^{-4}$, and $(0.6 \pm 0.2 \pm 0.2) \times 10^{-4}$. The inclusive branching ratio was $B(J/\psi \rightarrow \gamma\phi\phi) = (7.6 \pm 0.7 \pm 0.5) \times 10^{-4}$ from decay mode (a).

The spins and parities of these structures were determined by observing the distribution of the angle between the decay planes of the two vector particles (χ) and the decay angle of one of the decay products of the vector with respect to the direction of flight of the vector in its rest frame ($\cos\theta$), *i.e.*, the helicity angle.^[4] Figure 3(a) shows the expected distributions of these angles for different spin parities and Fig. 3(b) shows these distributions for the 2200 MeV/c² and the $\eta_c(2980)$ region. Both regions exhibit clear behavior like that expected for a pseudoscalar.

$J/\psi \rightarrow \gamma K^*(892)^0 \bar{K}^*(892)^0$

The $K^*(892)^0[\bar{K}^*(892)^0]$ decay was observed in the $K^+\pi^-$ ($K^-\pi^+$) final state. The reconstructed spectrum shown in Fig. 4 exhibits interesting structures including the $\eta_c(2980)$. A preliminary analysis shows all the regions to be pseudoscalar like from the χ angle and the helicity angle distributions. Fitting the spectrum with three Breit-Wigner amplitudes and the $\eta_c(2980)$, one obtains the parameters

of the structures as $M_1 = 1930 \pm 8 \pm 5 \text{ MeV}/c^2$, $\Gamma_1 = 75 \pm 19 \pm 10 \text{ MeV}/c^2$, $M_2 = 2067 \pm 11 \pm 5 \text{ MeV}/c^2$, $\Gamma_2 = 113 \pm 28 \pm 10 \text{ MeV}/c^2$, $M_3 = 2353 \pm 27 \pm 15 \text{ MeV}/c^2$, $\Gamma_3 = 180 \pm 50 \pm 40 \text{ MeV}/c^2$ and $M_{\eta_c} = 2986 \pm 4 \pm 4 \text{ MeV}/c^2$, $\Gamma_{\eta_c} = 24 \pm 8 \pm 8 \text{ MeV}/c^2$, respectively. The corresponding branching ratios measured are $(5.3 \pm 1.0 \pm 0.8) \times 10^{-4}$, $(6.2 \pm 1.3 \pm 0.9) \times 10^{-4}$, $(3.3 \pm 0.9 \pm 0.5) \times 10^{-4}$, and $(1.0 \pm 0.3 \pm 0.25) \times 10^{-4}$ for the three structures and the $\eta_c(2980)$, respectively.

$$\underline{J/\psi \rightarrow \gamma\pi^+\pi^-\pi^+\pi^-}$$

The effective mass spectrum of the four charged pions from a preliminary analysis are presented in Fig. 5(a). A small peak at $\sim 1285 \text{ MeV}/c^2$ corresponding to the $f_1(1285)$ production and a distinct peak at $2980 \text{ MeV}/c^2$ corresponding to the $\eta_c(2980)$ production are observed. The χ and the $\cos\theta$ distribution of the events from the $1285 \text{ MeV}/c^2$ region, shown in Fig. 6, follows the expected distribution of spin parity 1^+ . The measured branching ratios for the $f_1(1285)$ and the $\eta_c(2980)$ production are $B[J/\psi \rightarrow \gamma f_1(1285)] \cdot [f_1(1285) \rightarrow \pi^+\pi^-\pi^+\pi^-] = (0.55 \pm 0.11 \pm 0.10) \times 10^{-4}$ and $B[J/\psi \rightarrow \gamma \eta_c(2980)] \cdot [\eta_c(2980) \rightarrow \pi^+\pi^-\pi^+\pi^-] = (1.50 \pm 0.13 \pm 0.30) \times 10^{-4}$, respectively.

The $\rho\rho$ mass spectrum and the $f_2(1270)f_2(1270)$ mass spectrum are presented in Figs. 5(b) and (c), respectively. Both figures show clear $\eta_c(2980)$ peaks. The χ and the $\cos\theta$ distribution of the events from the η_c regions are pseudoscalar like and are not included here. The measured branching ratios for the $\eta_c(2980)$ production are $B[J/\psi \rightarrow \gamma \eta_c(2980)] \cdot [\eta_c(2980) \rightarrow \rho\rho] = (0.96 \pm 0.15 \pm 0.22) \times 10^{-4}$ and $B[J/\psi \rightarrow \gamma \eta_c(2980)] \cdot [\eta_c(2980) \rightarrow f_2(1270)f_2(1270)] = (1.2 \pm 0.3 \pm 0.4) \times 10^{-4}$. These two decay modes almost saturate the $\eta_c(2980)$ branching ratio into $\pi^+\pi^-\pi^+\pi^-$. The lower mass region of the $\rho\rho$ spectrum has structures very similar to those observed by the DM2 collaboration,^[5] and likewise exhibit pseudoscalar nature. These are presently under study.

$J/\psi \rightarrow \gamma\omega\phi$

Details of the analysis of this doubly OZI violating decay have been presented before.^[6] No $\eta_c(2980)$ signal was observed. An upper limit of $B[J/\psi \rightarrow \gamma\eta_c(2980)] \cdot [\eta_c(2980) \rightarrow \omega\phi] < 1.3 \times 10^{-5}$ was obtained at a 90% CL. The inclusive branching ratio of this decay mode was measured as $B(J/\psi \rightarrow \gamma\omega\phi) = (1.40 \pm 0.25 \pm 0.28) \times 10^{-4}$, corresponding to the few events observed. Six events were observed at the $\xi(2230)$ and, conservatively, an upper limit was calculated as $B[J/\psi \rightarrow \gamma\xi(2230)] \cdot [\xi(2230) \rightarrow \omega\phi] < 5.9 \times 10^{-5}$, at 90% CL.

$J/\psi \rightarrow \gamma\omega\omega$

This reaction was analysed and published with half the present data sample.^[7] It is now being updated with the complete statistics. The noticeable feature in the $\omega\omega$ mass distribution was a prominent broad structure above the threshold, of pseudoscalar nature. The inclusive branching ratio was measured as $B(J/\psi \rightarrow \gamma\omega\omega) = (17.6 \pm 0.9 \pm 4.5) \times 10^{-4}$, where the branching ratio for the broad structure, for $m_{\omega\omega} < 2 \text{ GeV}/c^2$, was $B(J/\psi \rightarrow \gamma\omega\omega) = (12.2 \pm 0.7 \pm 3.1) \times 10^{-4}$. No signal was observed at the $\eta_c(2980)$; an upper limit of $B[J/\psi \rightarrow \gamma\eta_c(2980)] \cdot [\eta_c(2980) \rightarrow \omega\omega] < 3.1 \times 10^{-5}$ was obtained at a 90% CL.

Figure 7 shows the vector vector channels for comparison (except $\omega\phi$, where statistics are low). All the channels exhibit broad pseudoscalar structures above the threshold. A coupled channel study to further investigate these structures are underway. The $\eta_c(2980)$ is clearly visible in $\phi\phi$, $K^*(892)^0\bar{K}^*(892)^0$ and $\rho\rho$. Table 1 compares the decay branching ratios of the $\eta_c(2980)$ from MARK III, DM2,^[8] and the expectations from SU(3) symmetry. The $\omega\omega$ mode seems to strongly violate SU(3). It is important to measure the $\omega\omega$ mode with full statistics.

3. SEARCH FOR SCALARS IN $J/\psi \rightarrow \gamma K^+ K^-$ AND $\gamma\pi^+ \pi^-$

The $f_2(1720)$ region in the decay modes $J/\psi \rightarrow \gamma\pi^+ \pi^-$ and $\gamma K^+ K^-$ have been discussed extensively at this conference.^[9] Only the search for scalars in the lower mass region will be discussed here.

$J/\psi \rightarrow \gamma\pi^+\pi^-$

The hadronic decay mode $J/\psi \rightarrow \rho\pi$, which has a large branching ratio,^[9] presents the largest source of background in the $\gamma\pi^+\pi^-$ mode, where one of the photons from the π^0 decay is not detected. Figure 8 shows the $\pi^+\pi^-$ mass spectrum where the dotted line represents the $\rho\pi$ background estimated from the $J/\psi \rightarrow \rho\pi$ data.^[10] The residual spectrum has a clear $f_2(1270)$ signal. A moment analysis was performed^[10] to the complete $\pi^+\pi^-$ mass range. After subtracting the $\rho\pi$ background, in the mass region of 500 to 900 MeV/c² no signal is observed, an upper limit of $B(J/\psi \rightarrow \gamma X) \cdot (X \rightarrow \pi^+\pi^-) < 3 \times 10^{-5}$ was obtained. Figure 9 displays the $\cos \theta_h$, $\cos \theta_\gamma$ and $|\phi_h - \pi|$ distribution of the events from the mass region between 300 and 500 MeV/c², where θ_h, θ_γ and ϕ_h are the polar angle of the pion in the helicity frame, polar angle of the radiative photon and the azimuthal angle of the pion in the helicity frame, respectively. The dotted curves are fit to the data for a $J^{PC} = 0^{++}$, *i.e.*, an s-wave, and an incoherent background from the decay $\rho^0\pi^0$. This is a good fit and we measure the following branching ratio: $B[J/\psi \rightarrow \gamma(\pi\pi)_{s\text{-wave}}] = (4.7 \pm 0.5 \pm 0.6) \times 10^{-5}$. We also obtain the following upper limit from a search for narrow peaks from 300 to 900 MeV/c², as $B(J/\psi \rightarrow \gamma X) \cdot (X \rightarrow \pi^+\pi^-) < 2.1 \times 10^{-5}$ at a 90% CL, and for the $f_0(975)$ production as $B[J/\psi \rightarrow \gamma f_0(975)] \cdot [f_0(975) \rightarrow \pi^+\pi^-] < 1.4 \times 10^{-5}$ at a 90% CL.

$J/\psi \rightarrow \gamma K\bar{K}$

Figure 10 presents the K^+K^- and the $K_S^0K_S^0$ final mass spectra. The charged mode, K^+K^- suffers from background similar to the $\pi^+\pi^-$ mode. The $K_S^0K_S^0$ mode is clean because the decay $J/\psi \rightarrow K_S^0K_S^0\pi^0$ is forbidden by C-parity violation, unlike the decay $J/\psi \rightarrow K^+K^-\pi^0$. The K^+K^- and the $K_S^0K_S^0$ spectra are very similar, which implies that the backgrounds are well understood. The $f_2'(1525)$ and the $f_2(1720)$ are clearly visible in both spectra. The moment analyses were performed to both decay modes. The presence of an s-wave like behavior was observed for events in the mass region between 1100 and 1400 MeV/c², in each mode. The branching ratios for the s-waves were measured as $B[J/\psi \rightarrow \gamma(K^+K^-)_{s\text{-wave}}] =$

$(1.7 \pm 0.1) \times 10^{-4}$ and $B[J/\psi \rightarrow \gamma(K_S^0 K_S^0)_{s\text{-wave}}] = (1.7 \pm 0.3) \times 10^{-4}$. A search for $a_0(980)$ yielded an upper limit $B[J/\psi \rightarrow \gamma a_0(980)] \times [a_0(980) \rightarrow K\bar{K}] < 2.9 \times 10^{-5}$ at a 90% CL.

4. HADRONIC DECAYS OF THE $J/\psi \rightarrow$ VECTOR TENSOR PAIR

The quark correlations and the various amplitudes, *e.g.*, the strong, electromagnetic, SU(3) violating, and the DOZI suppressing, have been determined for the hadronic decays of the J/ψ into a vector and a pseudoscalar pair^[9] by extensive measurements of the various decay modes. A similar study has been undertaken for the J/ψ hadronic decays into a vector tensor pair.

$J/\psi \rightarrow \omega f_2(1270)$

-The ω was observed in three pion decay and the $f_2(1270)$ in $\pi^+\pi^-$ decay. Figure 11 displays the Dalitz plot for the $\omega\pi^+\pi^-$ events, where $m_{\omega\pi^-}^2$ vs. $m_{\omega\pi^+}^2$ are plotted. Two bands are observed in the $\pi^+\pi^-$ mass distribution. A broad band near the low $\pi^+\pi^-$ mass boundary and a second band, the $f_2(1270)$, at a higher $\pi^+\pi^-$ mass, are observed. Two other bands, parallel to the axes are also observed, corresponding to the $b_1(1235)$ production (the isovector member of the $J^{PC} = 1^{+-}$ nonet). Because $b_1(1235)\pi$ and $\omega f_2(1270)$ share the same final state, events in the overlapping region, *i.e.*, containing a $b_1(1235)$ were removed. Figure 12 displays the projection of the $\pi^+\pi^-$ mass distribution (recoiling against an ω), with the $b_1(1235)$ removed. The low mass enhancement has previously been observed but has not been identified. The solid curve is the result of a fit to the data with a relativistic d-wave Breit-Wigner amplitude for the $f_2(1270)$, a three body phase space term to describe the nonresonant events and a combination of an exponential and a power term to describe the low mass enhancement. The mass and the width of the $f_2(1270)$ were $M = 1275 \pm 3 \text{ MeV}/c^2$ and $\Gamma = 174.1 \pm 11.7 \text{ MeV}/c^2$, and the branching ratio $B[J/\psi \rightarrow \omega f_2(1270)] = (39 \pm 2 \pm 5) \times 10^{-4}$ *. This should

* An amplitude analysis of the events from the $\omega f_2(1270)$ region were performed to calculate the efficiency with the involved angular distribution and to test the amount of resonant $\omega f_2(1270)$ contribution. The results were in agreement with the above measurements.

be compared with the results of the DM2 collaboration, $B[J/\psi \rightarrow \omega f_2(1270)] = (40 \pm 6) \times 10^{-4}$.

$J/\psi \rightarrow \rho a_2(1320)$

This reaction was measured^[11] in all three charged modes; the final states in each case were $\eta\pi^+\pi^-\pi^0$. The branching ratio was measured to be $B[J/\psi \rightarrow \rho a_2(1320)] = (112 \pm 9 \pm 19) \times 10^{-4}$.

A search for the isospin violating decay $J/\psi \rightarrow \omega a_2(1320)$ was made, and an upper limit $B[J/\psi \rightarrow \omega a_2(1320)] < 2.3 \times 10^{-4}$ was obtained. Another isospin violating reaction, $J/\psi \rightarrow \rho f_2(1270)$, is being analyzed. Preliminary results of the decay modes $J/\psi \rightarrow \phi f_2'(1525)$, $J/\psi \rightarrow K^*(892)^0 \overline{K}^*(1430)^0 + cc$ have been presented^[11] at various conferences. A complete amplitude analysis of the decay mode $J/\psi \rightarrow \phi f_2'(1525)$, which takes into account the possible interference with the $f_2(1720)$, is almost completed. A similar detailed analysis of the reaction $J/\psi \rightarrow K^*(892)^0 \overline{K}^*(1430)^0 + cc$ is underway.

In the scalar sector, a coupled channel analysis of $f_0(975)$ from the decay modes $J/\psi \rightarrow \phi\pi^+\pi^-$ and $J/\psi \rightarrow \phi K^+K^-$ is also close to completion. Preliminary results of the analysis have previously been presented. An attempt to study the reaction $J/\psi \rightarrow \rho a_0(980)$ was made in the $\eta\pi^+\pi^-\pi^0$ final states; the same final states in which the decay mode $\rho a_2(1320)$ was observed. Since no signal of this reaction was observed, an upper limit $B[J/\psi \rightarrow \rho a_0(980)] < 4.4 \times 10^{-4}$ was obtained at a 90% CL.^[12]

In summary, the MARK III continues to be a rich ongoing program, with many new and interesting results, and many more yet to come. The J/ψ provides a clean and important laboratory to search and study glueballs, hybrids and meson spectroscopy, as seen from the results of the MARK III and DM2 experiments.

REFERENCES

1. K. Ishikawa *et al.*, *Phys. Rev. C* **19**, 327 (1983); B. A. Berg *et al.*, *Phys. Rev. Lett.* **57**, 400 (1986); T. A. De Grand, *Phys. Rev. D* **36**, 176 (1987) and references therein.
2. T. H. Burnett, in these proceedings.
3. D. G. Hitlin, in these proceedings.
4. N. P. Chang and C. T. Nelson, *Phys. Rev. Lett.* **40**, 1617 (1978); T. L. Trueman, *Phys. Rev. D* **18**, 3423 (1978).
5. D. Bisello *et al.*, LAL-88-12, June 1988, submitted to *Phys. Rev. D*.
6. J. J. Becker *et al.*, contributed paper to the XXIII International Conference on High Energy Physics, Berkeley, California, 1986.
7. R. M. Baltrusaitis *et al.*, *Phys. Rev. Lett.* **55**, 1723 (1985).
8. L. Stanco, Invited Talk at the 1987 International Europhysics Conference on High Energy Physics, Uppsala, Sweden, June-July 1987.
9. D. Coffman *et al.*, to appear in *Phys. Rev. D*, SLAC-PUB-4424; Z. Azaltouni *et al.*, LAL-88-06, April 1988.
10. T. A. Bolton, Ph.D. thesis (unpublished).
11. U. Mallik, Proceedings of the SLAC Summer Institute, Stanford, California, June-July 1986; SLAC-PUB-4238 (1987).
12. W. Lockman, Invited Talk at the Topical Seminar on Heavy Flavors, San Miniato, Italy, September 1987.

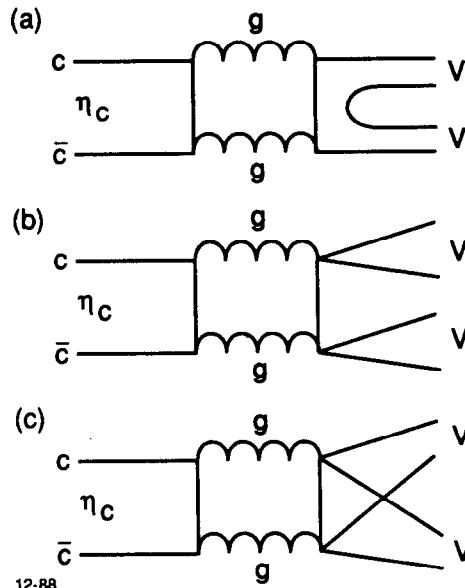
FIGURE CAPTIONS

1. The decay mechanisms of the $\eta_c(2980)$ into vector vector.
2. Reconstructed $\phi\phi$ mass spectrum from the decay mode, where: (a) both ϕ 's decay into K^+K^- ; and (b) one ϕ decays into K^+K^- and the other ϕ decays into $K_S^0K_L^0$, after correcting for the efficiency. The dotted line depicts the efficiency.
3. (a) The expected distributions of the χ angle and the helicity angles for different spin parities; and (b) the χ angle and $\cos(\theta)$ distributions from the 2200 MeV/c² and the $\eta_c(2980)$ regions, not corrected for efficiencies.
4. The reconstructed $K^*(892)^0\bar{K}^*(892)^0$ mass spectrum, corrected for efficiency. - The dotted line shows the efficiency.
5. (a) The effective $\pi^+\pi^-\pi^+\pi^-$ mass distribution; (b) the reconstructed $\rho\rho$ mass distribution, a subset of (a); and (c) the reconstructed $f_2(1270)f_2(1270)$ mass distribution, a subset of (a).
6. The χ and the $\cos(\theta)$ distribution of the events from the region 1250 to 1300 MeV/c². The dashed lines show the expected distributions for spin parity 1^+ . The dotted lines show the expected distributions for spin parity 0^- .
7. The radiative vector vector decay modes of the J/ψ for comparison. The reconstructed mass distribution of (a) $\phi\phi$ (efficiency corrected); (b) $K^*(892)^0\bar{K}^*(892)^0$; (c) $\omega\omega$ (half the statistics); and (d) $\rho\rho$.
8. Final $\pi^+\pi^-$ mass spectrum with $\rho\pi$ background estimate (dots).
9. The $\cos(\theta_h)$ (θ_h , the helicity angle of one of the pions), $\cos(\theta_\gamma)$ (θ_γ , the polar angle of the radiative photon), and $|\phi_h - \pi|$ (ϕ_h , the azimuthal angle of the pion in the helicity frame) distributions of events in the mass region between 300 and 500 MeV/c². The dotted lines are the fit to the data, assuming the J^{PC} of the events to be 0^{++} .

10. The K^+K^- and $K_S^0K_S^0$ mass spectra.
11. The Dalitz plot distribution of the $\omega\pi^+\pi^-$ events, $m_{\omega\pi^-}^2$ vs. $m_{\omega\pi^+}^2$. The diagonal bands represent structures in $\pi^+\pi^-$ mass distribution.
12. The $\pi^+\pi^-$ mass distribution of the events recoiling against an ω , with $b_1(1235)$ removed. The resultant dark solid line represents a fit with a d-wave relativistic Breit-Wigner parametrization of the $f_2(1270)$ signal with the combination of an exponential and a power term, and a three-body phase space to describe the low mass enhancement and the background.

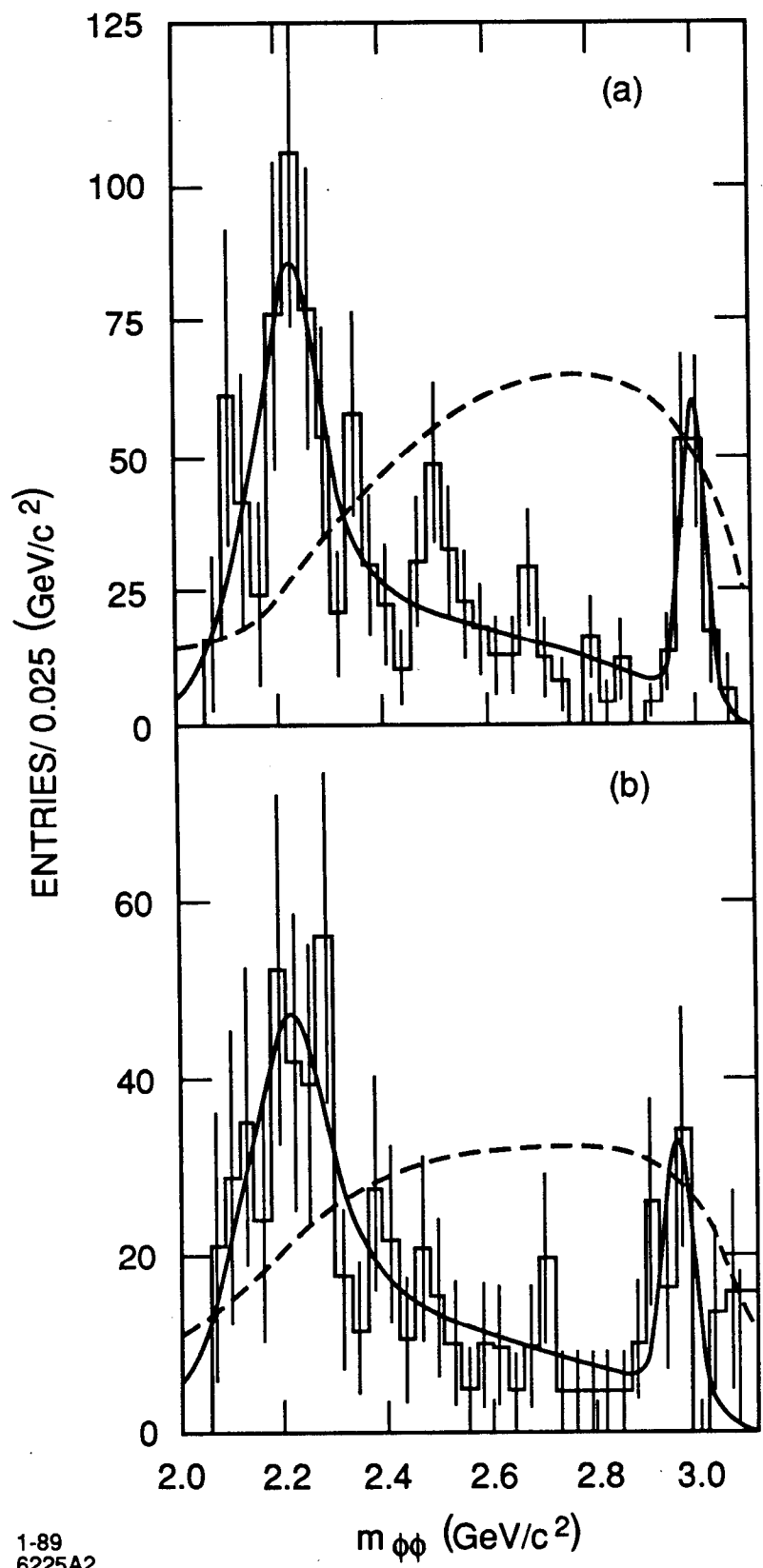
Table 1: $\eta_c(2980)$ Branching Ratios

Decay Mode	Branching Ratio $\times 10^{-4}$		SU(3) Prediction with phase space corr.
	MARK III	DM2	
$(J/\psi \rightarrow \eta_c) \times$			
$\eta_c \rightarrow \phi\phi$	$0.96 \pm 0.2 \pm 0.14$ $0.6 \pm 0.2 \pm 0.2$	$0.39 \pm 0.09 \pm 0.09$	1
$\eta_c \rightarrow$ $K^*(892)^0 \bar{K}^*(892)^0 + cc$	$1.0 \pm 0.3 \pm 0.25$	0.55 ± 0.18	1.3×2
$\eta_c \rightarrow \rho^0 \rho^0$	$0.96 \pm 0.15 \pm 0.22$	$0.87 \pm 0.26 \pm 0.13$	1.6
$\eta_c \rightarrow \omega\phi$	< 0.13		0
$\eta_c \rightarrow \omega\omega$	< 0.31	< 0.8	1.6



12-88
6225A1

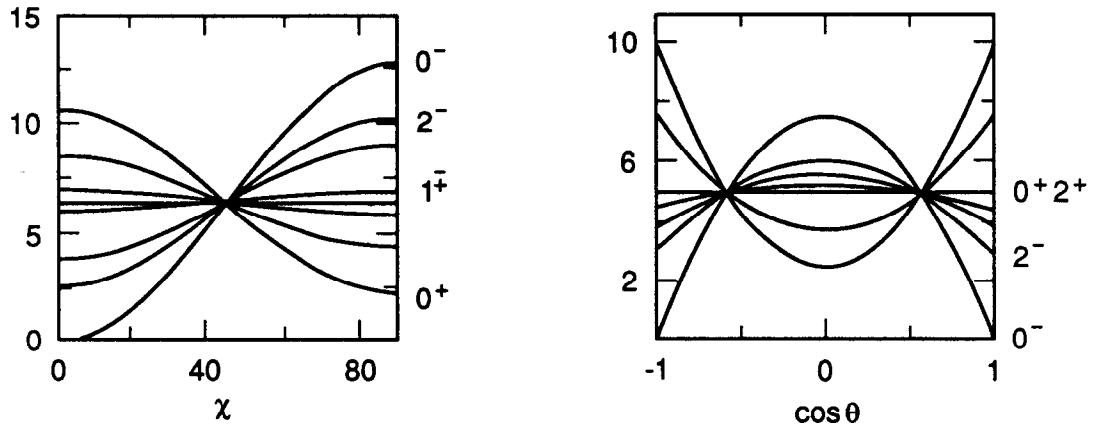
Fig. 1



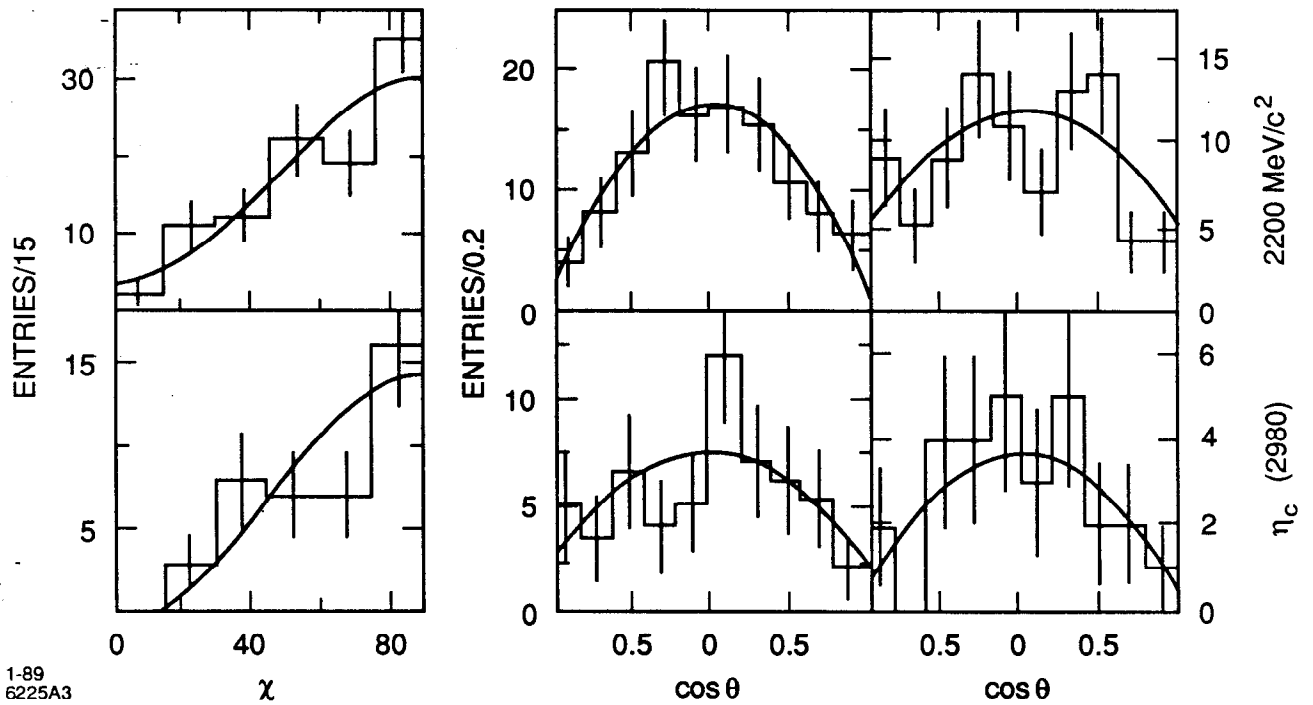
1-89
6225A2

Fig 2

(a)



(b)



1-89
6225A3

Fig. 3

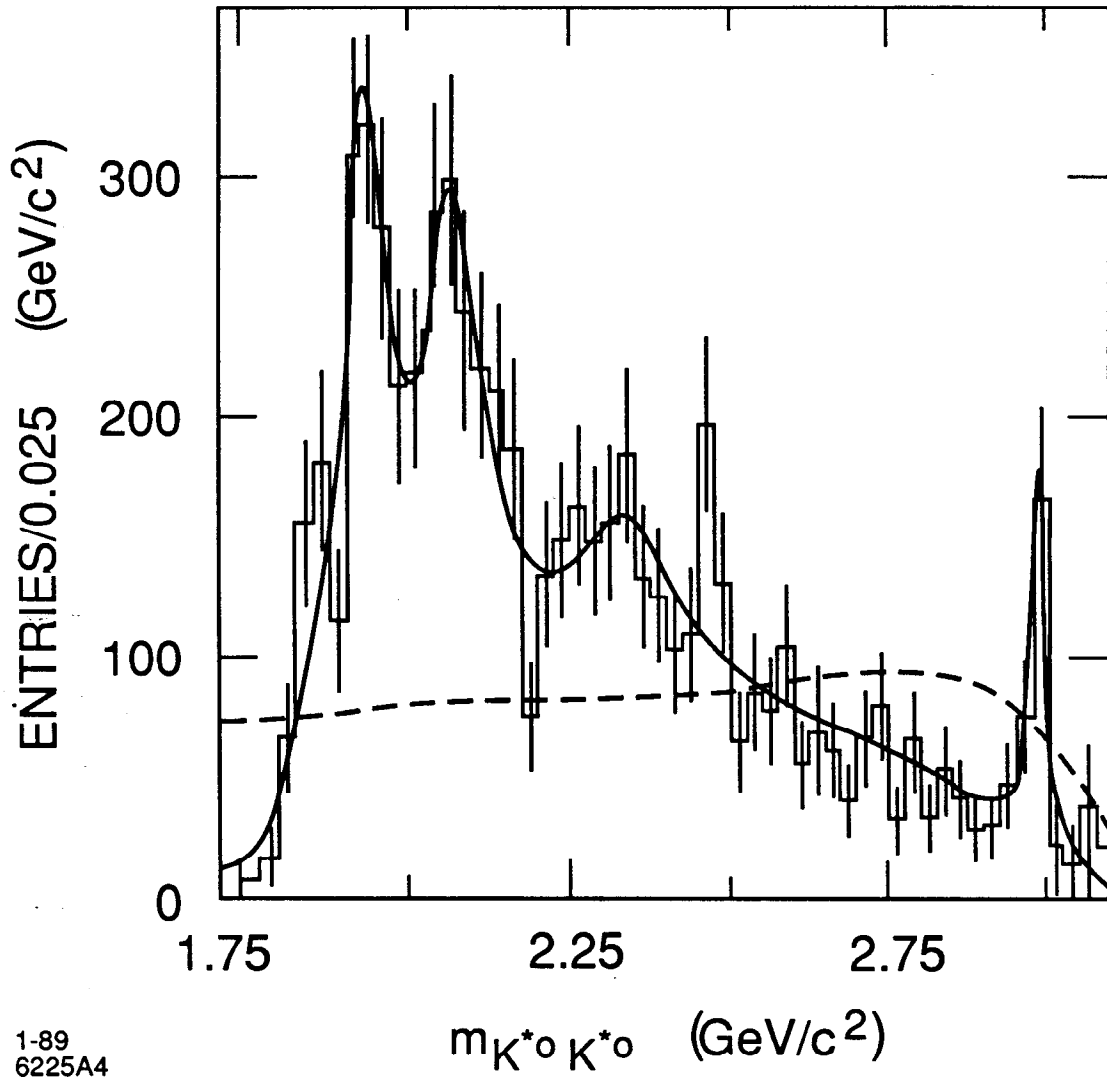


Fig. 4

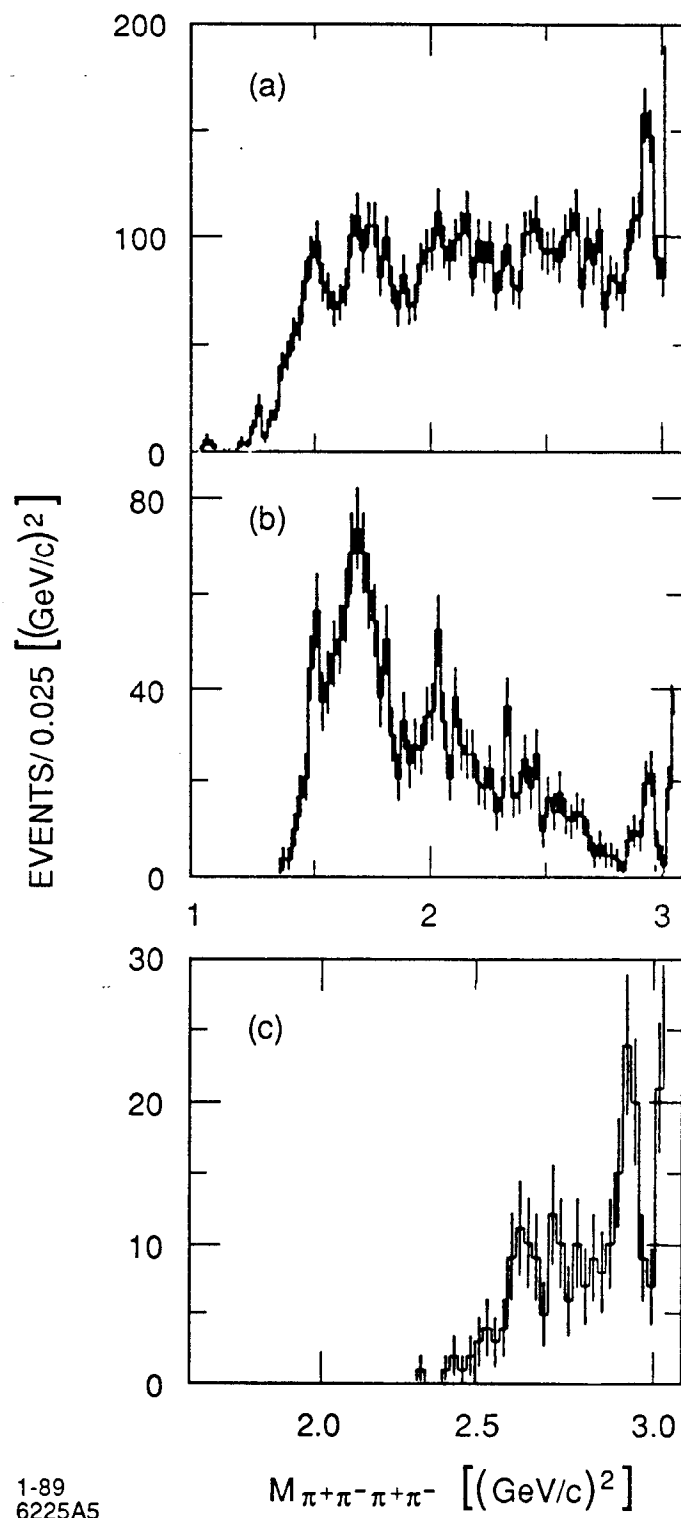
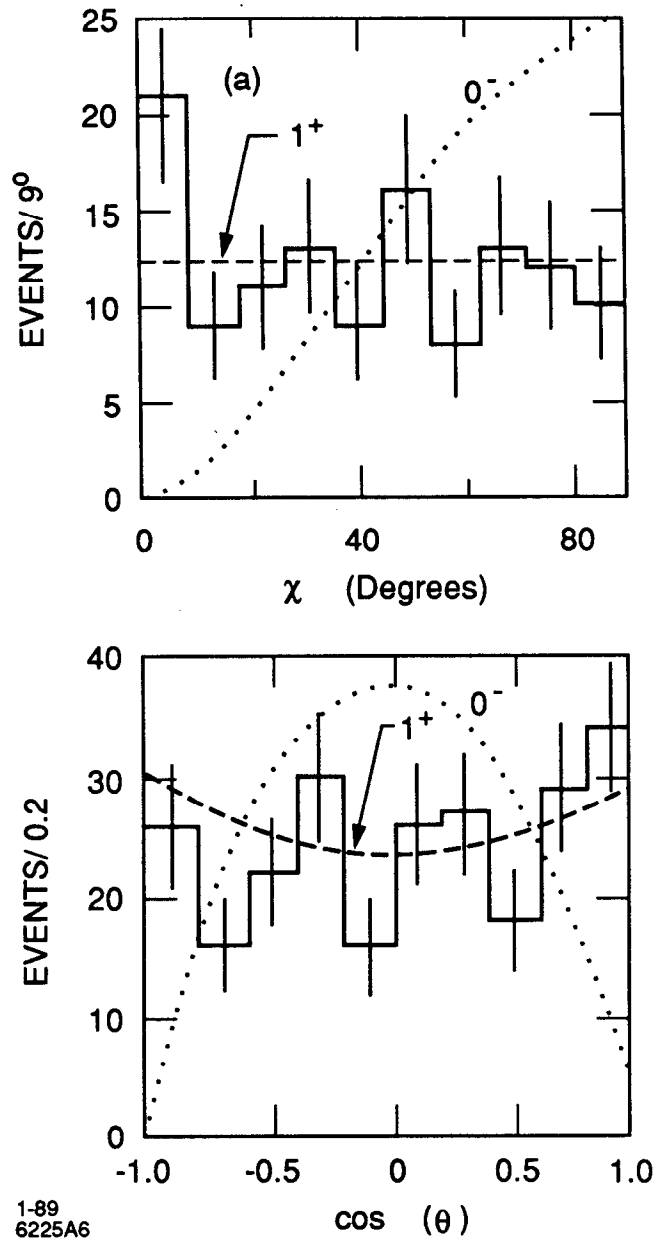
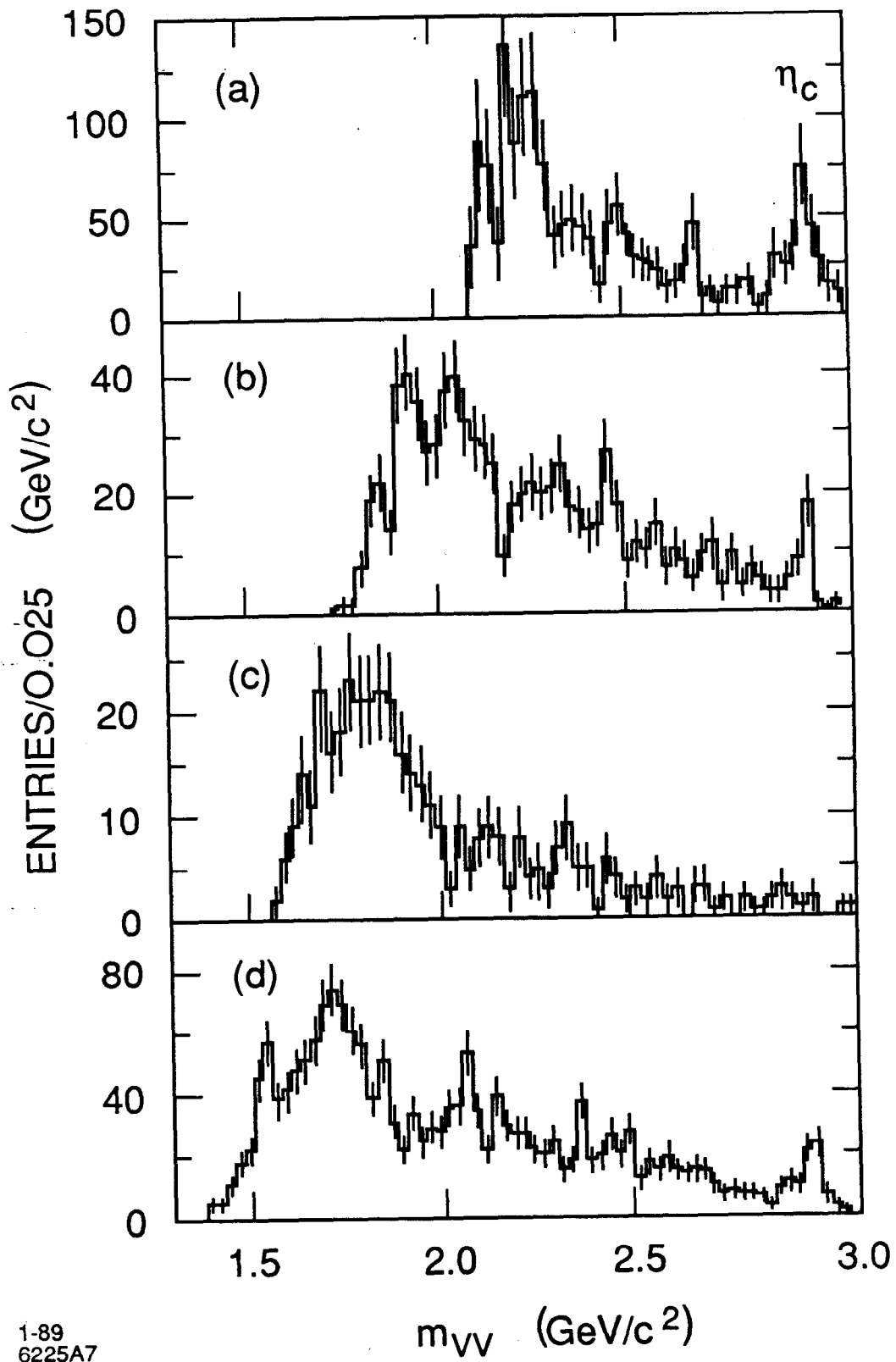


Fig. 5



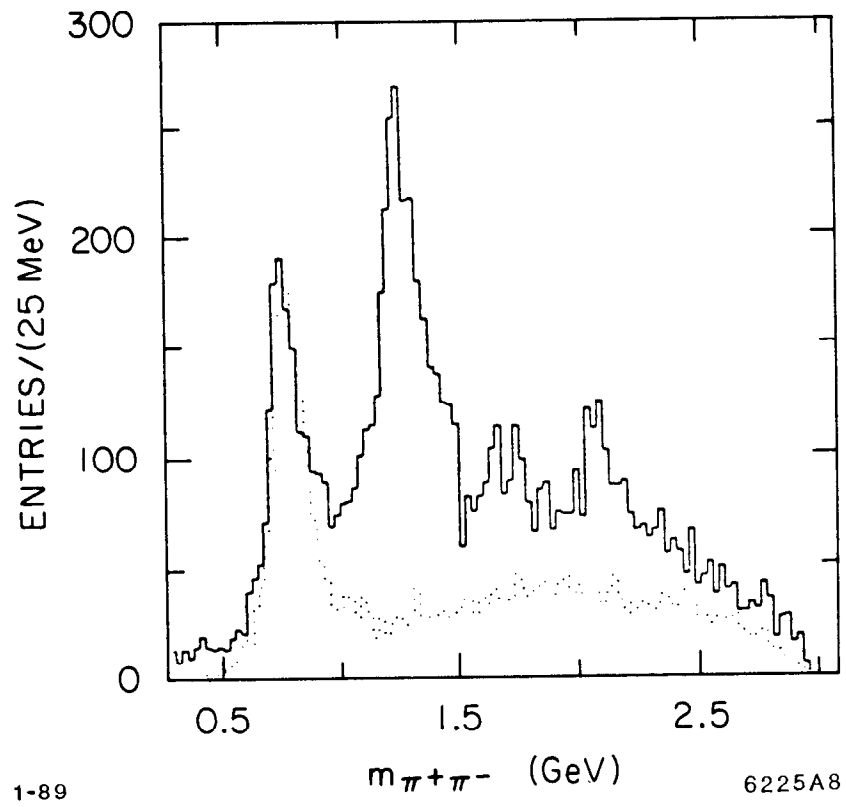
1-89
6225A6

Fig. 6



1-89
6225A7

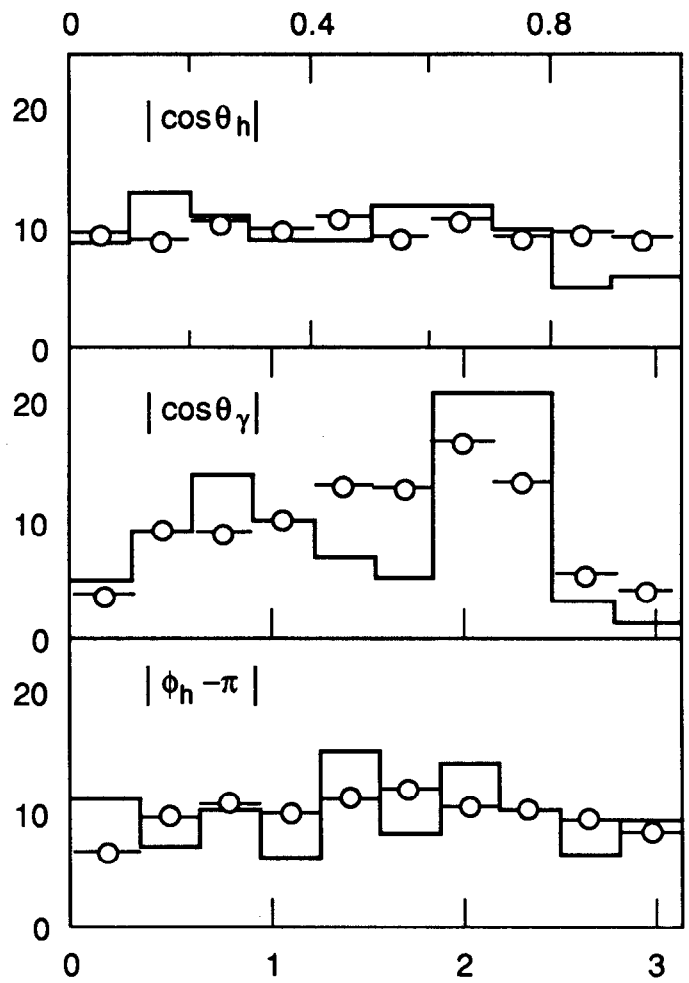
Fig. 7



1-89

6225A8

Fig. 8



6225A9

1-89

Fig. 9

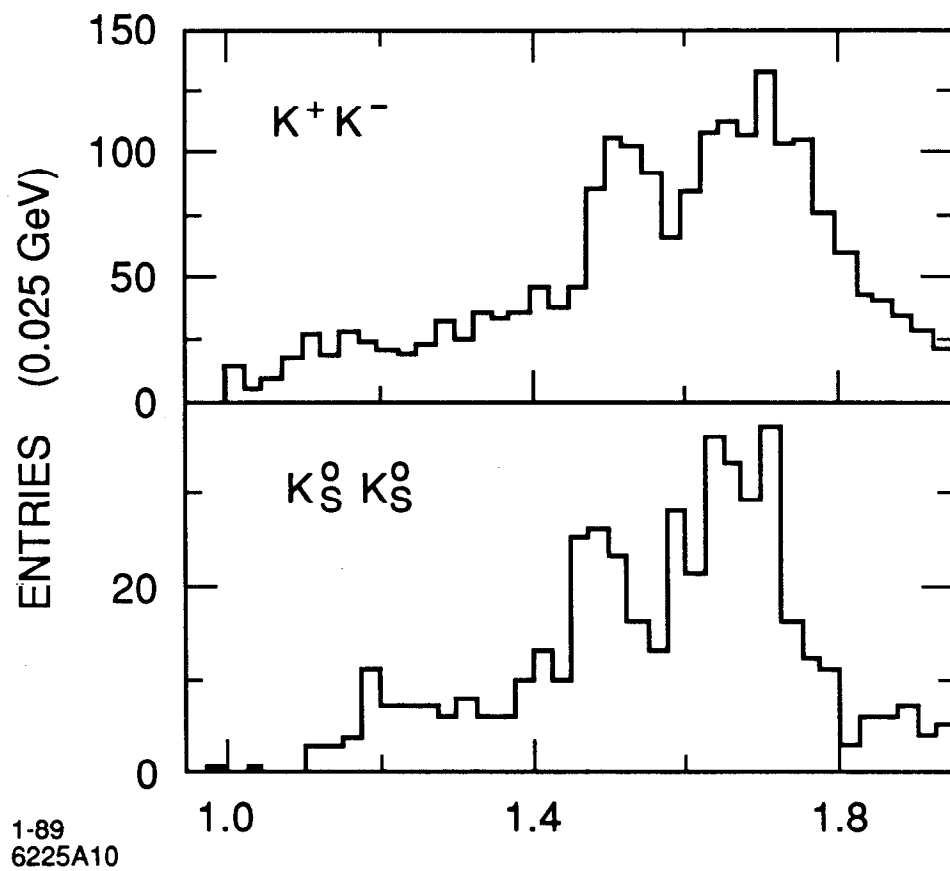


Fig. 10

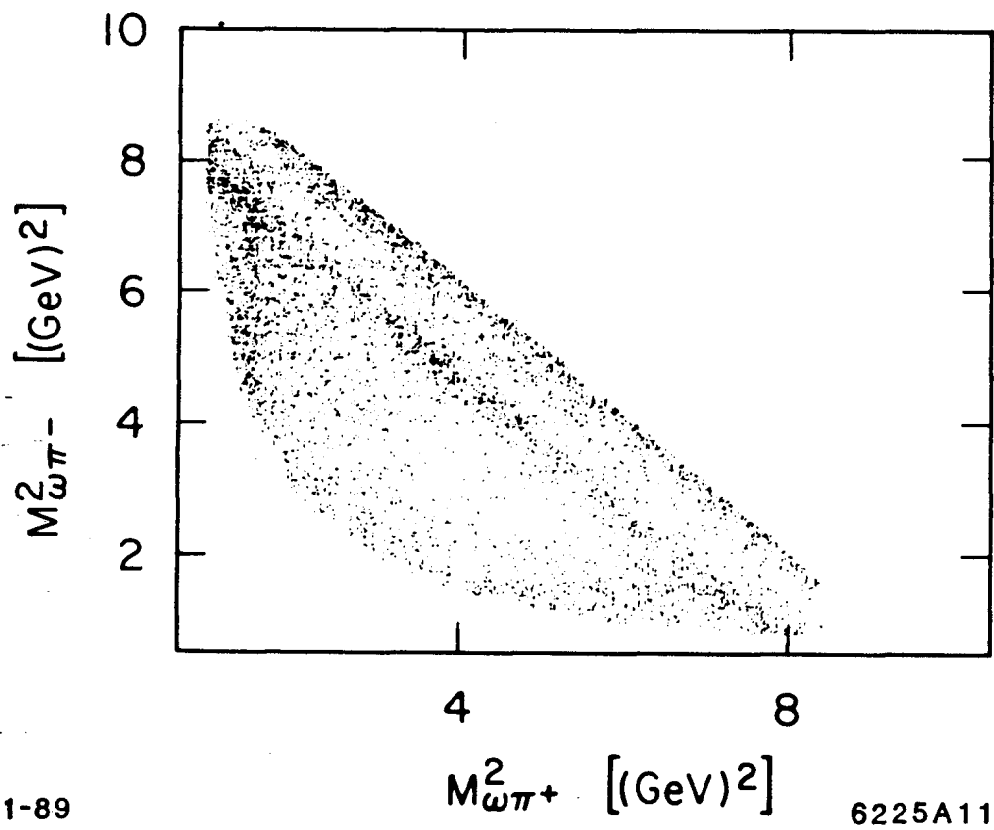


Fig. 11

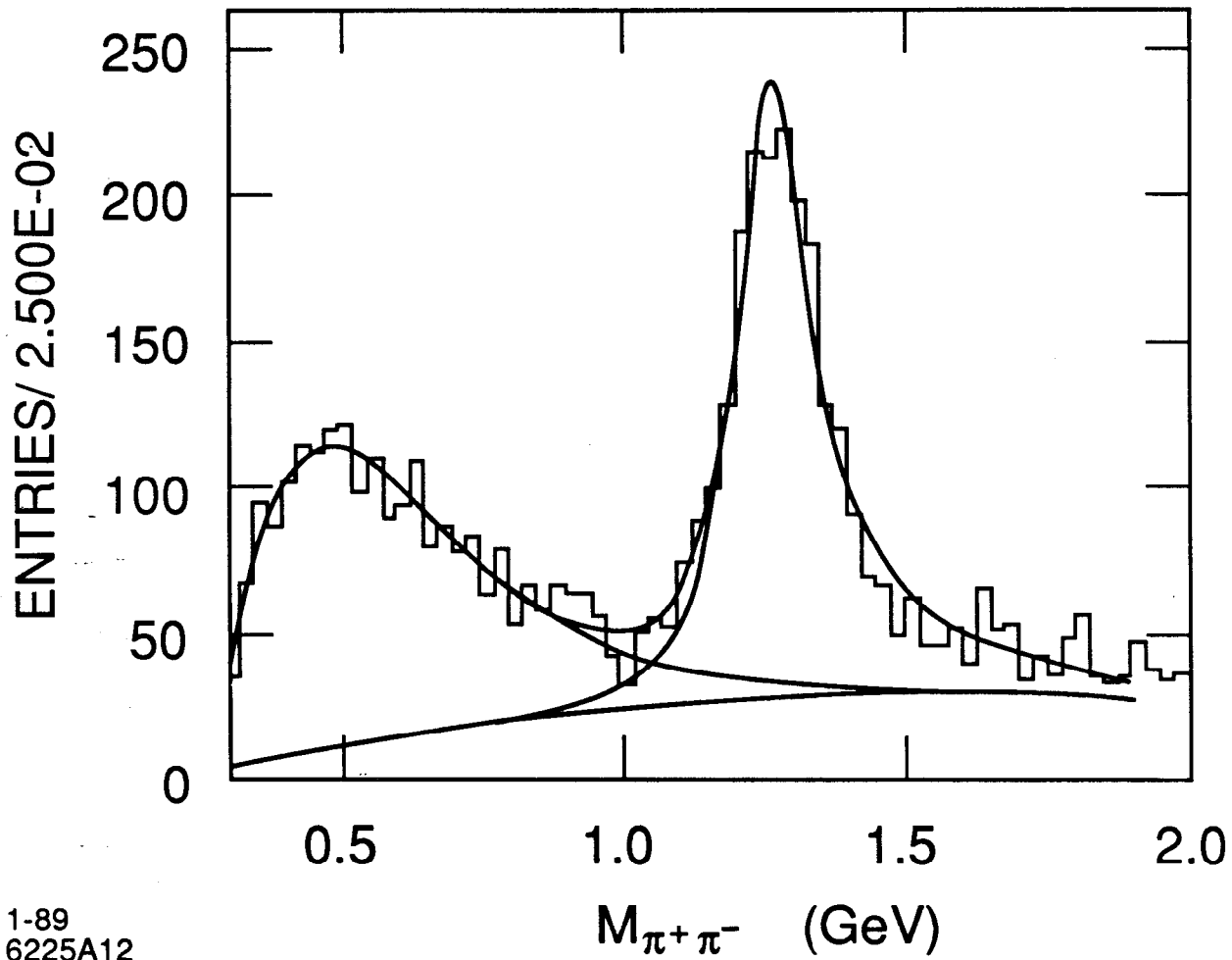


Fig. 12